# Magnesium and calcium silicate hydrates, Part II Mg-exchange at the interface “low-pH” cement and magnesium environment studied in a C-S-H and M-S-H model system

E. Bernard, Alexandre Dauzères, B. Lothenbach

# Accepted Manuscript

Magnesium and calcium silicate hydrates, part II: Mg-exchange at the interface “low-pH” cement and magnesium environment studied in a C-S-H and M-S-H model system

Ellina Bernard, Alexandre Dauzères, Barbara Lothenbach

PII: S0883-2927(17)30370-0

DOI: 10.1016/j.apgeochem.2017.12.006

Reference: AG 4001

To appear in: *Applied Geochemistry*

Received Date: 11 July 2017

Revised Date: 4 December 2017

Accepted Date: 5 December 2017

Please cite this article as: Bernard, E., Dauzères, A., Lothenbach, B., Magnesium and calcium silicate hydrates, part II: Mg-exchange at the interface “low-pH” cement and magnesium environment studied in a C-S-H and M-S-H model system, *Applied Geochemistry* (2018), doi: 10.1016/j.apgeochem.2017.12.006.

# Magnesium and calcium silicate hydrates, Part II: Mg-exchange at the interface "low-pH" cement and magnesium environment studied in a C-S-H and M-S-H model system

Ellina Bernard[1)*], Alexandre Dauzères[2)], Barbara Lothenbach[1)]

[1)] Empa, Laboratory for Concrete & Construction Chemistry, 8600 Dübendorf, Switzerland

[2)] IRSN, Institute of Radiation Protection and Nuclear Safety, PSE/SEDRE/LETIS, BP 17, 92262 Fontenay aux Roses, France

*Corresponding author: Bernard E., email: ellina.bernard@empa.ch

## Abstract

"Low-pH" cementitious materials have been developed in the context of nuclear wastes encapsulation to reduce the alkaline plume and the early hydration heat causing shrinkage of the Portland cement based-materials in contact with clayey rocks. This study follows the evolutions at an interface between calcium silicate hydrate (C-S-H) with a Ca/Si ratio of 0.8 and magnesium silicate hydrate (M-S-H) with a Mg/Si ratio of 0.8, while controlling the pore solution by using reservoirs. In a first step a simplified "low-pH" binder was mimicked by C-S-H with a low Ca/Si in the presence of magnesium. In a second step the impact of calcium on pure M-S-H was studied. Secondary electron microscopy observations show the fast deterioration of the C-S-H and the precipitation of M-S-H in the C-S-H disk and an uptake of calcium in the M-S-H disk together with a change of the reservoir compositions including pH values. The reactive transport modelling is in good agreement with the changes in both the solid phases and the composition of the solution reservoirs.

**Keywords**

Low-pH cement, interface, calcium silicate hydrate (C-S-H), magnesium silicate hydrate (M-S-H), scanning electron microscopy (SEM), reactive transport modelling

## 1. Introduction

The pore solution of the Portland cement is highly alkaline with a pH greater than 13. This high pH value can lead to alterations in the surrounding clayey rocks in underground repositories as envisaged for nuclear wastes (Berner, 1992). To reduce the alkaline plume of concrete, so called “low-pH” concretes have been developed, e.g. (Cau Dit Coumes et al., 2006; Codina, 2007; Codina et al., 2008; Lothenbach et al., 2012; Lothenbach et al., 2014), which contain in addition to Portland cement, pozzolanic materials such as silica fume, fly ash or slag. Such “low-pH” cement pastes are mainly composed of calcium silicate hydrate (C-S-H) and ettringite. The presence of silica-rich minerals lowers the Ca/Si ratio in C-S-H to 0.7-1.2 as well as the pH, such that the pH values after 3 months of hydration range from 10.5 to 12 (Bach et al., 2013; Codina, 2007; Codina et al., 2008; Hong and Glasser, 1999; Lothenbach et al., 2012; Poyet et al., 2014). Although “low pH” cement pastes have significantly lower pH values than Portland cement, mineralogical changes still occur at the interfacial zone with the host rock (Dauzères et al., 2016; Garcia Calvo et al., 2010; Jenni et al., 2014). Leaching and carbonation of the cement paste by ground water lowers the pH values at the interface, decalcifies the C-S-H and releases amorphous silica. Also, the precipitation of ettringite and calcite is observed due to higher concentrations of sulfates and carbonates in the ground water in equilibrium with the rocks (Dauzères et al., 2014; Garcia Calvo et al., 2010; Jenni et al., 2014; Pearson et al., 2003). In addition, the precipitation of magnesium-bearing phase at the interface has been detected due to the presence of magnesium in the interstitial solutions of the “host” rocks or swelling clays (Dauzères et al., 2016; Fernández et al., 2017;

Garcia Calvo et al., 2010; Jenni et al., 2014; Lerouge et al., 2017; Mäder et al., 2017). At the interfaces of low pH concretes and Opalinus clayey rock (OPA) a poorly crystalline phase containing magnesium and silicon with a sheet-like structure was observed in association with C-S-H (Dauzères et al., 2016; Lerouge et al., 2017; Mäder et al., 2017). Reactive transport modelling and experimental observations indicate tentatively the formation of magnesium silicate hydrate (M-S-H) (Dauzères et al., 2016). However the proof of M-S-H formation and the study of their properties is complicated by the presence of clay minerals from OPA as M-S-H has a similar sheet structure as clay minerals.

Based on electron microprobe and EDS in TEM and other complementary techniques, it has recently been suggested that M-S-H is a tri-octahedral 2:1 phyllosilicate containing not only magnesium and silicate, but also some aluminum, calcium and iron comparable to a (Ca, Mg) smectite (Lerouge et al., 2017).

Even though several papers might pointed towards the existence of a magnesium silicate hydrate phase at the interface, proof of M-S-H formation and the study of their properties is complicated by the presence of clay minerals, which have the same silicate sheet structure as M-S-H. Thus the present paper focuses on the characterization of the changes occurring at the interface of C-S-H and M-S-H only, using a simplified model system and is the part II of a study on the stability and the uptake of the magnesium and calcium silicate hydrates. In the first paper (Bernard et al., submitted), the uptake of magnesium by C-S-H and calcium by M-S-H was investigated and the small uptake of calcium in M-S-H has been confirmed in batch experiments.

This work aims at investigating the formation of M-S-H in similar conditions as in field experiments (Dauzères et al., 2016; Jenni et al., 2014; Lerouge et al., 2017; Mäder et al., 2017), by experimenting a simplified model system. Previous batch experiments gave the evidence of the coexistence of M-S-H

and C-S-H (Bernard et al., submitted; Bernard et al., 2017a; Lothenbach et al., 2015). Recently, it was demonstrated that a low amount of calcium can be taken up by M-S-H, while no magnesium uptake in C-S-H was observed (Bernard et al., submitted). It was also observed that pH values lower than 10 and/or the addition of magnesium destabilized C-S-H (Bernard et al., 2017a). The present study focuses on the evolution of a simplified interface between pure C-S-H and pure M-S-H in an experimental setup which allows studying the changes in the solid phases and in the pore solutions, using SEM/EDS and FTIR analyses of solids, the chemical compositions of solutions and the reactive transport modelling.

## 2. Materials and methods

### 2.1. Synthesis

M-S-H and C-S-H have been synthetized as detailed in (Bernard et al., submitted; Bernard et al., 2017b). The syntheses were performed in a glovebox under nitrogen atmosphere to minimize $CO_2$ contamination and carbonation processes. MgO, CaO and $SiO_2$ were directly mixed with ultrapure water to obtain C-S-H with Ca/Si = 0.8 or M-S-H with Mg/Si = 0.8 at a water to solid ratio (W/S) of 45. The suspensions were equilibrated for 3 months at 50°C to accelerate the synthesis (Bernard et al., 2017b), separated by filtration using pressure filtration system (4-5 bar $N_2$) and nylon filters (0.45 µm). After the filtration, the solids were washed with a 50/50 (volume) water-ethanol mix and then with ethanol (94 wt% alcohol) to remove dissolved ions and to prevent the precipitation of salts during drying. The samples were freeze-dried with liquid nitrogen (for approximatively 20 min at -195°C) and kept at -40°C under vacuum at ~0.28 mbar for 7 days. The solid phases were analyzed after further equilibration in $N_2$-filled desiccators at a relative humidity of ~30% (saturated $CaCl_2$ solution) for a period of 14 days or longer (up to 2 months) to ensure ~30% RH in all the samples.

After drying, the samples were gently ground by hand and the M-S-H and C-S-H powders were compacted and shaped into disks (32 mm by diameter, 2.0 ± 0.2 cm by height, resulting in a total weight of 2.2 g and 1.6 g for C-S-H and M-S-H, respectively) using a mechanical press. Based on the apparent density measured by helium pycnometry of 2.3 and 2.0 g/cm$^3$ for C-S-H and M-S-H, a total porosity 50-60% was estimated.

The applied force depended on the materials (10kN for C-S-H and 5kN for M-S-H). C-S-H powder was easy to compact, while preparing M-S-H disks was very challenging due to its poor cohesion. The relatively poor compacting of the M-S-H disk and the resulting high porosity will not affect the alterations but will fasten transport within the cell. The disks were mounted and fixed together using a resin (a mix 50:50 mix of Resoltech 3037 and 3030) in the cell as shown in Figure 1. Finally, the reservoirs on each side were filled with 125 mL of solution at equilibrium with the respective material which has been collected during the filtration of the synthesized C-S-H and M-S-H. The experiments were allowed to equilibrate either for 3 or for 12 months at 25°C before they were dismantled and the solid and liquid phase was analyzed.

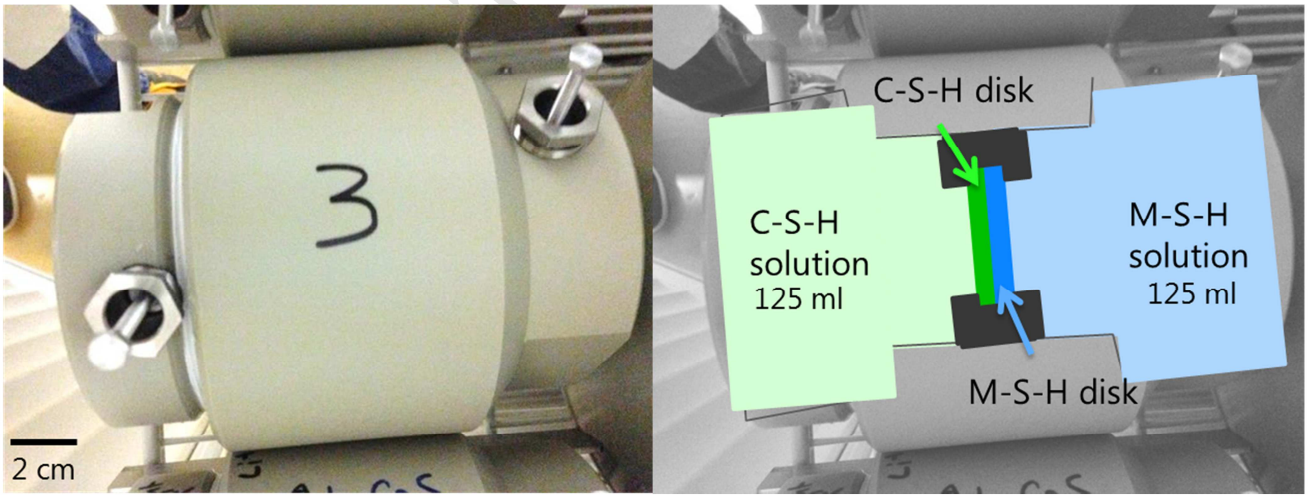


*Figure 1: Interface experiment in the diffusion cell, picture and schematic sketches.*

## 2.2. Analytical techniques

The chemical composition of the solutions was analysed by ion chromatography (IC). The dissolved concentrations of Mg, Ca, Si, Na, Cl, K, $SO_4$ in undiluted solutions or in solutions diluted by factors of 10, 100 or 1000 were quantified using a Dionex DP serie ICS-3000 ion chromatography system. Silicon was analyzed using sodium carbonate/bicarbonate eluent and sodium molybdate, and sodium lauryl sulfate in metasulfonic acid as a post-column reagent using an ion pack AS22 column. All concentrations have been determined as duplicate and the mean is given, measurement error $\leq$ 10%.

The pH (±0.1) was measured at ambient temperature (23±2°C) in an aliquot of the reservoirs and the measured pH values were corrected to 25°C.

The cell was dismantled after 3 or 12 months. The interface was cut in two pieces; one was embedded with an epoxy resin to maintain the sample during the sample preparation for the SEM characterizations, the second part was kept for further analysis.

The scanning electron microscopy (SEM) characterizations were carried out on a SEM Hitachi in high vacuum mode under a 15 kV voltage. The semi-quantification of Mg, Si, Ca, C by energy dispersive spectrometry (EDS) was done by two Bruker SDD EDS detectors with a spot size of 1 to 3 μm. The working distance used for elementary mappings was 16 mm and the duration of map acquisition about 25 minutes. Observations were performed on a polished section coated with carbon for chemical analyses. The EDS measurements were calibrated by measuring Cu. 300 to 500 EDS analyses were carried out on M-S-H and C-S-H disks after 3 months and 1000 EDS analyses after 12 months. Note that initially the M-S-H disk and C-S-H disk were completely free of calcium or magnesium respectively.

In the other part of the sample some material was scratched off by hand at the interface and in the sound C-S-H and M-S-H disk to be analyzed by attenuated total reflectance (ATR) Fourier Transformation-

Infrared (FTIR). FTIR was used to identify C-S-H, M-S-H and/or M-(C)-S-H as well as the formation of other hydrates or carbonates within the samples. The FTIR spectra were recorded in the mid-region on a Bruker Tensor 27 FT-IR spectrometer between 600 and 4000 $cm^{-1}$ with a resolution of 4 $cm^{-1}$ by transmittance on small amounts of powder. Spectra were background corrected and scaled to the maximum of Si-O bonds to ease comparison. The spectrum recorded on a synthetic M-(C)-S-H (Mg/Si=0.75, Ca/Si=0.05) from (Bernard et al., submitted) was used as reference.

### 2.3. Reactive transport modelling

The HYTEC reactive transport code (Van der Lee, 1998; Van Der Lee et al., 2003) was used to reproduce the chemical changes and model the interactions between the C-S-H and the M-S-H disks and in the surrounding solutions.

HYTEC takes into account geochemistry and physical parameters variations due to mineralogical changes in the solid. The HYTEC code solves the chemical-transport problem by coupling CHESS chemical equilibrium code with a R2D2 transport module.

The transport equation of a chemical species in water saturated media can be written as:

$$\frac{\partial \omega C_i^{sol}}{\partial t} = div\left(D * \overrightarrow{grad}.\, C_i^{sol}\right) - \frac{\partial \omega C_i^{p}}{\partial t}$$

where ω is the porosity, $C_i^{sol}$ the mobile fraction in the chemical component $C_i$ , $C_i^{p}$ the immobile fraction incorporating component $C_i$ (precipitate), and $D$ the effective diffusion coefficient.

In the present case all calculations were performed at thermodynamic equilibrium with the Newton-Raphson iterative method, taking into account: minerals, solutions, aqueous and gaseous species. In the present modelling, the effect of precipitation and dissolution on porosity and the effect of diffusion coefficient were not used for the sake of simplicity.

A one-dimension system was used for the present simulation. The reservoirs, the C-S-H and the M-S-H disks were represented by successive rectangles. The volume of each zone was representative of the experimental conditions. A zero flux condition was imposed on the right and the left border. The mesh-size was equal to 20 µm in the disks and a progressive meshing was imposed in the reservoir (between 100 and 500 µm). The modelling aimed rather at assessing whether the formation of Mg-phases was possible in the C-S-H disk and not at reproducing perfectly the extension of the disturbance front. Only the places where chemical changes occurred were of interest, while the transport properties of the disks were of minor interest and an effective diffusion coefficient of $2.10^{-11}$ $m^2/s$ was assumed for both the C-S-H and M-S-H disks.

The thermodynamic data used for modelling are given in Table 1. The equilibrium constants were recalculated to the master species used in CHESS i.e. $SiO_2$, $Mg^{2+}$, $Ca^{2+}$, $H_2O$, and $H^+$. As the available solid-solution models for C-S-H (Kulik, 2011), M-S-H (Bernard et al., 2017b) and M-(C)-S-H (Bernard et al., submitted) cannot be directly implemented in CHESS, 4 different C-S-H phases (Ca/Si=0.67, 0.80, 1.00 and 1.50) and 5 M-S-H phases (without calcium: Mg/Si=0.78, 0.83, 1.00 and 1.30; with calcium: Mg/Si=0.78 and Ca/Si=0.05) were defined instead and introduced in the database. The use of several solubility products instead of a continuous solid solution allows reproducing the general trends of the solid and the liquid phase compositions, although stepwise instead of continues changes occur (Bernard et al., 2017b; Kulik, 2011; Lothenbach et al., 2015; Nied et al., 2016; Walker et al., 2016).

The experiments, the SEM observations and the modelling were carried out in the LUTECE lab (IRSN) while the FTIR spectra were measured at Empa.

*Table 1: Standard thermodynamic properties at 25 °C.*

| | | Log Kf | Réf. |
|---|---|---|---|
| Brucite | $Mg^{2+} + 2H_2O \rightarrow Mg(OH)_2 + 2H^+$ | -17.12 | (Hummel et al., 2002) |

| | | | | |
|---|---|---|---|---|
| M-S-H | Mg/Si = 0.78 | $0.78Mg^{2+}+SiO_2 + 2.26\ H_2O \rightarrow (MgO)_{0.78}.SiO_2.(H_2O)_{1.48} + 1.56H^+$ | -7.25 | (Bernard et al., 2017b) |
| M-S-H | Mg/Si = 0.83[a] | $0.83Mg^{2+} + SiO_2 + 2.33\ H_2O \rightarrow (MgO)_{0.83}.SiO_2.(H_2O)_{1.50} + 1.66H^+$ | -7.90 | Adp.(Bernard et al., 2017b) |
| M-S-H | Mg/Si = 1.00[a] | $Mg^{2+} + SiO_2 + 2.60\ H_2O \rightarrow MgO.SiO_2.(H_2O)_{1.60} + 2H^+$ | -10.43 | Adp.(Bernard et al., 2017b) |
| M-S-H | Mg/Si = 1.30 | $1.3Mg^{2+} + SiO_2 + 3.1\ H_2O \rightarrow (MgO)_{1.30}.SiO_2.(H_2O)_{1.8} + 2.6H^+$ | -14.96 | (Bernard et al., 2017b) |
| M-(C)-S-H | Mg/Si = 0.78 Ca/Si = 0.05[b] | $0.78Mg^{2+} + 0.05Ca^{2+} + SiO_2 + 2.33\ H_2O \rightarrow (MgO)_{0.78}(CaO)_{0.05}.SiO_2.(H_2O)_{1.5} + 1.66H^+$ | -7.92 | Adp.(Bernard et al., submitted; Bernard et al., 2017b) |
| C-S-H | Ca/Si = 0.67[c] | $0.67Ca^{2+} + SiO_2 + 2.34\ H_2O \rightarrow (CaO)_{0.67}.SiO_2.(H_2O)_{1.67} + 1.34H^+$ | -8.29 | Adp.(Kulik, 2011) |
| C-S-H | Ca/Si = 0.80[c] | $0.8Ca^{2+} + SiO_2 + 2.74\ H_2O \rightarrow (CaO)_{0.8}.SiO_2.(H_2O)_{1.94} + 1.6H^+$ | -10.60 | Adp.(Kulik, 2011) |
| C-S-H | Ca/Si = 1.00 | $Ca^{2+} + SiO_2 + 3\ H_2O \rightarrow (CaO).SiO_2.(H_2O)_2 + 2H^+$ | -12.15 | (Kulik, 2011) |
| C-S-H | Ca/Si = 1.50 | $1.5Ca^{2+} + SiO_2 + 4\ H_2O \rightarrow (CaO)_{1.5}.SiO_2.(H_2O)_{2.5} + 3H^+$ | -25.39 | (Kulik, 2011) |
| $SiO_2$ | amorphous | $SiO_2\ (aq) \rightarrow SiO_2\ (am)$ | 2.71 | (Hummel et al., 2002) |

[a] *single phases adapted from (Bernard et al., 2017b)*
[b] *single phase adapted from (Bernard et al., submitted): the Ca/Si has been set lower than the end-members proposed in (Bernard et al., submitted) as Ca/Si of 0.10 has never been observed experimentally nor in the modelling*
[c] *single phase adapted from (Kulik, 2011).*

# 3. Results

## 3.1. Experiments

### 3.1.1. Solid analysis

The changes at the interface between the C-S-H and the M-S-H disk were studied by SEM/EDS. The SEM scattering electrons picture of the interface after 12 months is presented in Figure 2a. An overview of the different zones where EDS quantifications were carried out is given in Figure 2b.

a)

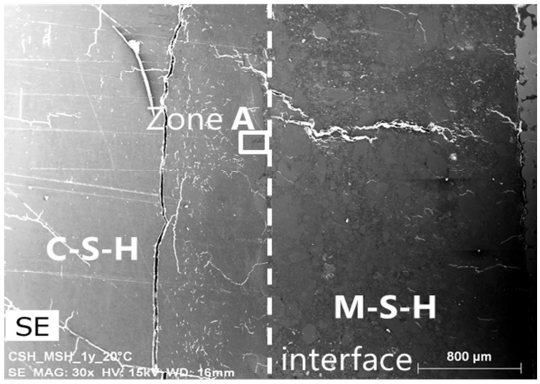


b)

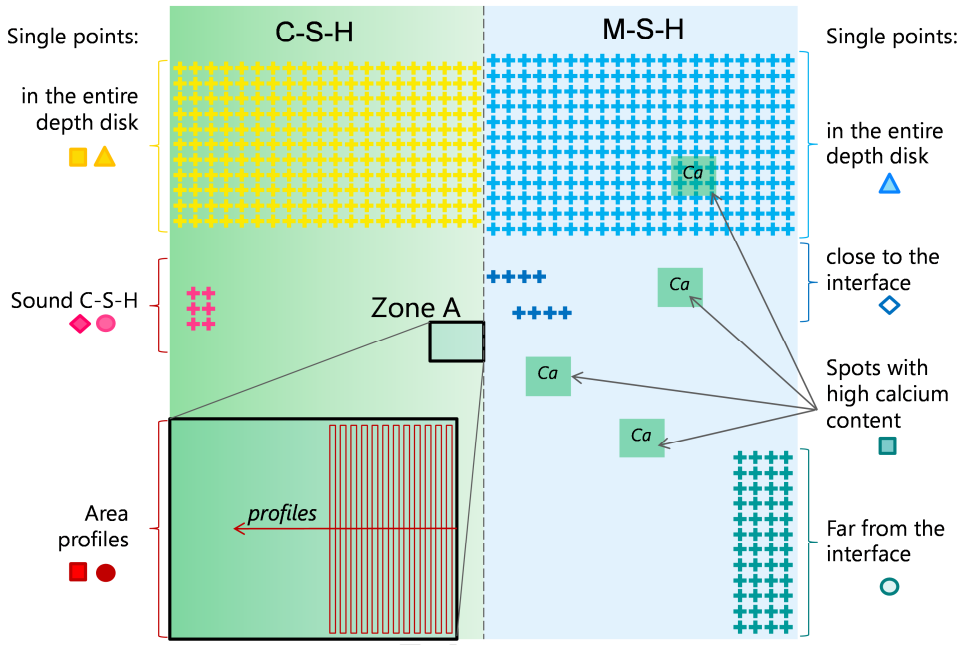


*Figure 2: a) SEM picture of the interface C-S-H and M-S-H disks after 12 months at 25°C, b) overview of the different zones where the composition has been determined by EDS quantifications. Depth=the distance from the interface; the symbols showed in this figure are used in the next figures to represent the results obtained in the different zones.*

### 3.1.1.1. C-S-H disk

The EDS mapping of the area near the interface (zoom A, Figure 2) after 3 and 12 months are presented in Figure 3a. Some cracks occurred after equilibration during the dismantling of the cells and due to the high vacuum used for SEM/EDS analysis. The C-S-H in some distance from the interface showed no evident changes except the occurrence of a few spots where calcium carbonate might have formed. FTIR

186 analysis on the scratched zone of sound C-S-H confirmed the presence of only C-S-H with a band at
187 ~964 $cm^{-1}$ assigned to Si–O stretching vibrations of the $Q^2$ tetrahedra and of a low amount of carbonates
188 with the carbonate bands at 1400–1500 $cm^{-1}$. Near the interface of the C-S-H with the M-S-H a
189 depletion of calcium was observed. After 3 month up to a depth of approximately 200μm; after 12
190 months this depletion of calcium reached 600 to 800 μm in depth. Also a depletion of silicon was
191 observed which extended to comparable depths. In the area where the calcium and silicon were depleted
192 the occurrence of some small crack filled by epoxy resin the near the interface were detected. The
193 carbon detected by SEM in the cracks was mainly due to the epoxy resin used to embed the interface.
194 However, possibly carbonates could also have formed in those cracks.

195 In addition a enrichment of magnesium was observed near to the interface at a depth of ~50-60 μm after
196 3 months and 200-220 μm after 12 months. The depth of the depletion of calcium and of magnesium
197 enrichment increased at least by a factor 4 between 3 and 12 months. The large difference in the depths
198 of decalcification and magnesium enrichment indicated that first the dissolution of C-S-H occurred and
199 only later the precipitation of M-S-H. These two steps are consistent with the different structures of C-S-
200 H, which contains silica chains, and M-S-H, which contains silica sheets (Bernard et al., 2017a; Brew
201 and Glasser, 2005; Lothenbach et al., 2015). Based on the EDS measurement it could not be decided
202 whether two phases (C-S-H and M-S-H) were present or whether some magnesium might had been
203 taken up in the C-S-H phase as the spot size was ~1 to 3 μm such that closely intermixed phases would
204 be captured in the same analysis. Uptake of magnesium in C-S-H however, seems little probable as
205 dedicated batch experiments have shown no measurable uptake of magnesium in C-S-H (Bernard et al.,
206 submitted). Although Figure 3a clearly shows a magnesium front in the C-S-H disk, only a small
207 fraction of the magnesium moved from the M-S-H disk to the C-S-H disk as visualized in Figure 3b
208 based on the relative intensity of magnesium of the M-S-H side.

The FTIR analysis of the C-S-H disk far from the interface and at the interface confirmed the presence of C-S-H plus a small amount of calcium carbonate. Additionally, some amorphous silica was observed at the interface with a band at 1190 $cm^{-1}$ and some shoulders related to M-S-H could be identified at 1100 $cm^{-1}$. The presence of only a weak shoulder indicating $Q^3$ characteristic of M-S-H at the interface (**Error! Reference source not found.**) indicates the presence of much less M-S-H than C-S-H in the sample scratched off the interface.

a) C-S-H: 3 months C-S-H: 12 months

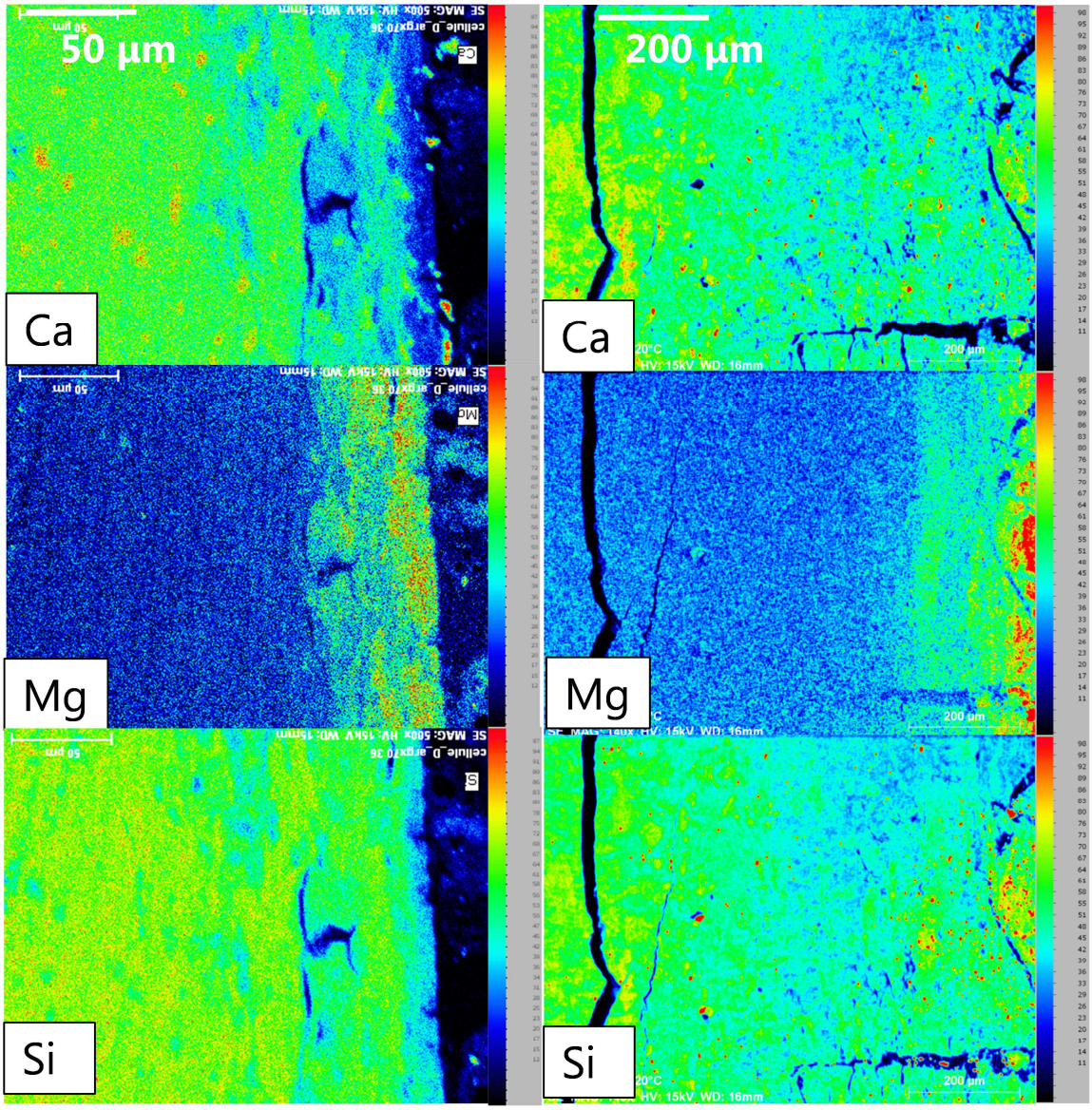


216

b) C-S-H: 12 months

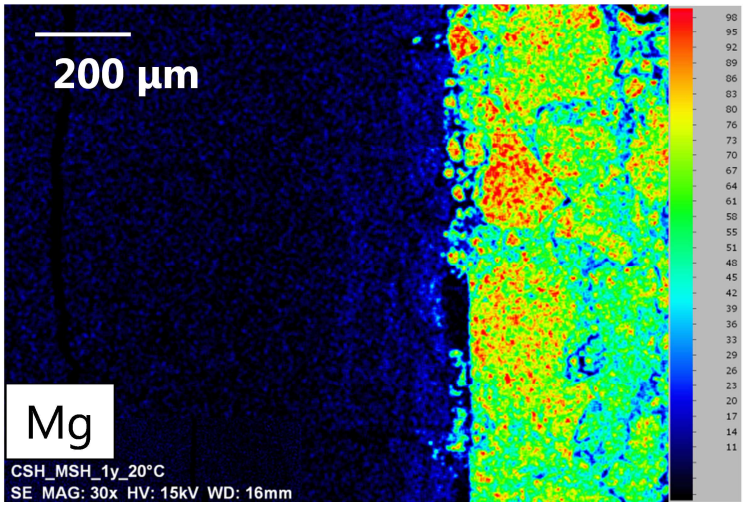


c) M-S-H: 3 months

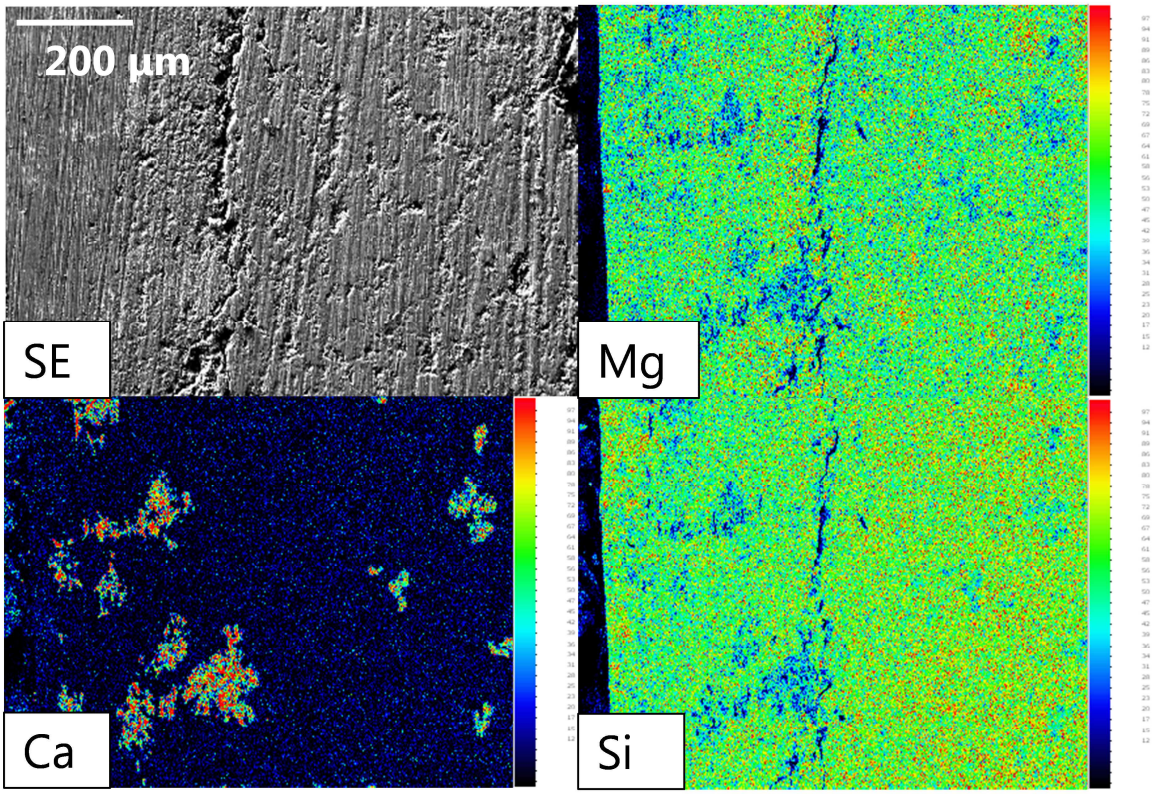


*Figure 3: a) EDS elemental mapping of the C-S-H near the interface (zoom A as detailed in Figure 2), b) magnesium enrichment in C-S-H compared to the M-S-H disk (colors were normalized to the lowest and the highest content) and EDS elemental mapping of M-S-H disk close to the interface (interface on the left).*

222 The $Ca/Si_{tot}$ and $Mg/Si_{tot}$ quantified by EDS are plotted as a function of the distance to the interface in
223 Appendix B. $Mg/Si_{tot}$ decreased from 0.4 at the interface to 0 far from the interface. Far from the
224 interface a Ca/Si= 0.8±0.1 was maintained but it decreased to $Ca/Si_{tot}$ of about 0.6±0.1 at the interface.
225 The EDS maps in Figure 3 illustrate that both the calcium but also the silicon moved away from the
226 interface between 3 and 12 months. However, as both calcium and silicon were depleted, a similar Ca/Si
227 was observed after 3 and 12 months in Appendix B.

228 The EDS data are summarized in a ternary diagram in Figure 4. The EDS points include C-S-H far from
229 the interface as well as C-S-H near the interface as detailed in Figure 2b. The composition of the C-S-H
230 far from the interface remained unchanged at Ca/Si = 0.8, although a bigger spread of the data (0.8 ±0.3)
231 was observed after 12 months. Nearer to the interface, a gradient in direction of M-S-H was visible
232 already after 3 months and much clearer after 12 months. As the spot size of the EDS analysis was ~1 to
233 3 μm such closely intermixed phases are captured in the same analysis resulting in many cases in mixed
234 analysis. In addition, a trend towards amorphous silica was observed after 12 months as well a few
235 points towards high calcium content. As in these small calcium rich areas very little and no silica or no
236 magnesium was observed, these points indicated that a small amount of calcium carbonate had formed
237 either during the interaction with M-S-H or during the drying and impregnation procedure. No trends
238 towards magnesium hydroxide or carbonate were visible indicating the absence of brucite or magnesite
239 in the C-S-H disk.

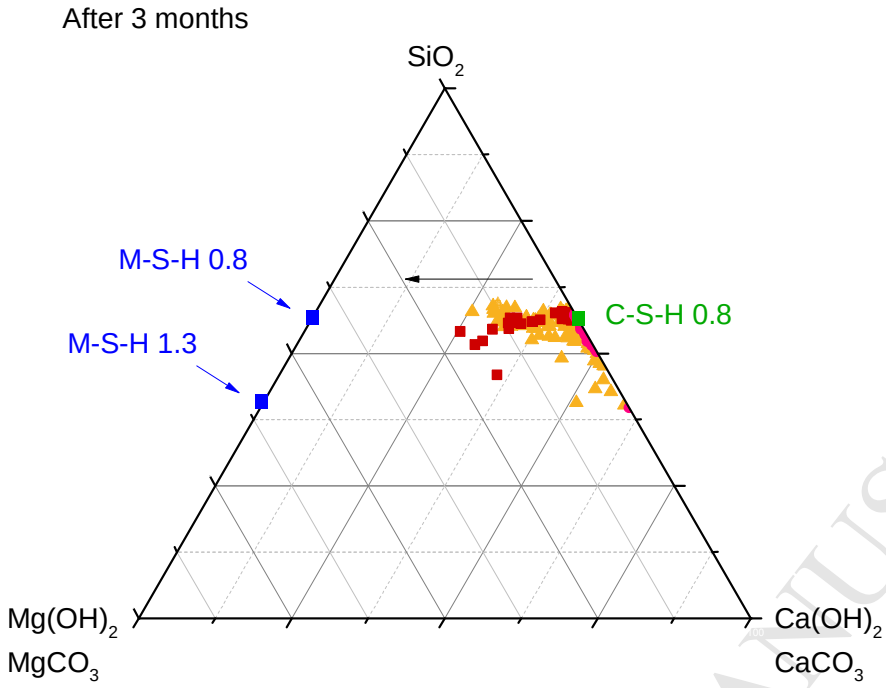


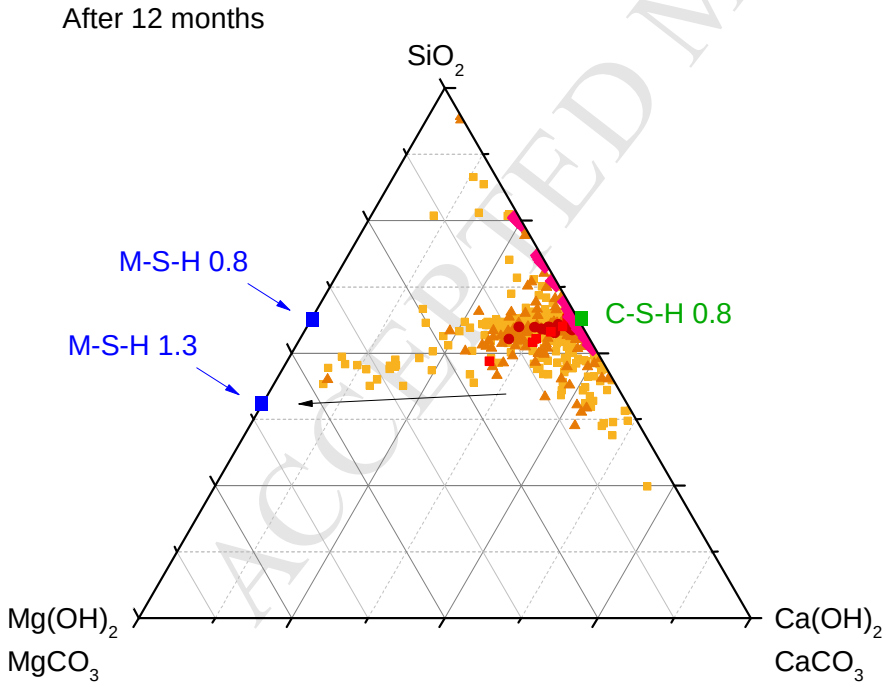


*Figure 4: Ca-Si-Mg ternary plots (in molar units) obtained from EDS measurements of the C-S-H disk after 3 and 12 months in contact with M-S-H. Yellow tringles and squares: singles points in the entire depth disks, red squares and red circles: area profiles, pink diamonds: far from interface C-S-H.*

#### 3.1.1.2. M-S-H disk

The analysis of the M-S-H disk focused on the 3 months results where a homogeneous M-S-H was prepared, as the disk analyzed after 12 months was not well compacted and was partially disintegrated already prior to exposure as shown in Figure 3b. Second electron images and the EDS mapping of the M-S-H disk are summarized in Figure 3c. In contrast to the C-S-H disk, no front was observed in the M-S-H disk and neither silicon nor magnesium were leached near the interface. The measured Mg/Si molar ratio (Figure 5) was found to vary between 0.8 to 0.6 independent from the distance to the interface.

The calcium distribution in the M-S-H was heterogeneous. Defined areas with high calcium content but no or very little silicon and magnesium are visible in Figure 3c, again indicating the presence of calcium carbonate in the samples, as also visible in the ternary diagram summarizing the EDS data in Figure 5a. A more detailed analysis, however, indicated that in all measurements a small amount of calcium was present in M-S-H as shown in Figure 5b. All measured points, even those far from the interface, contained calcium, and the Ca/Si varies between 0.03 to 0.08 as shown in Figure 5b, although initially no calcium had been present (Ca/Si = 0).

The FTIR analysis of the M-S-H disk (**Error! Reference source not found.**) showed almost identical spectra independently of the depth in the M-S-H disk. A much lower carbonation than in the C-S-H disk is observed and the spectra are similar to the spectrum of M-(C)-S-H (Mg/Si=0.75, Ca/Si=0.05).

The calcium uptake could either be due to finely and homogeneously distributed calcite intermixed with M-S-H or more probably due to an uptake of some calcium in M-S-H. In fact, the uptake of some calcium on the negatively charged M-S-H has been observed in dedicated batch experiments (Bernard et al., submitted). Calcium (together with aluminum and iron) had also be observed in M-S-H collected from the interface between clays and cement (Lerouge et al., 2017).

A few EDS data measured on the M-S-H disk after 12 months are also represented in Figure 5. Similar results, Mg/Si (0.8 ±0.1) and Ca/Si (0.07 ±0.02), were obtained even if the mean values of the two ratio were slightly higher after 12 months.

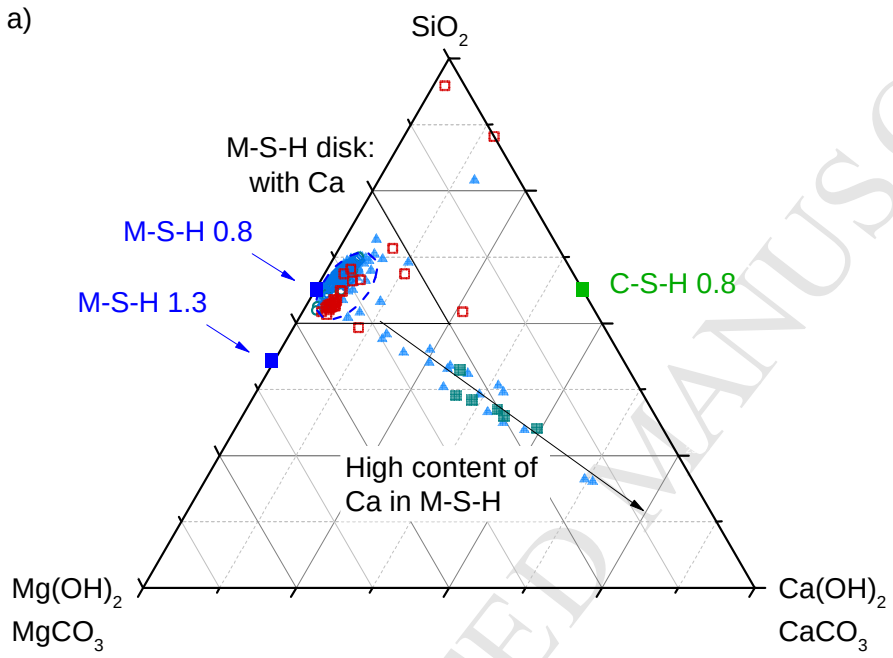

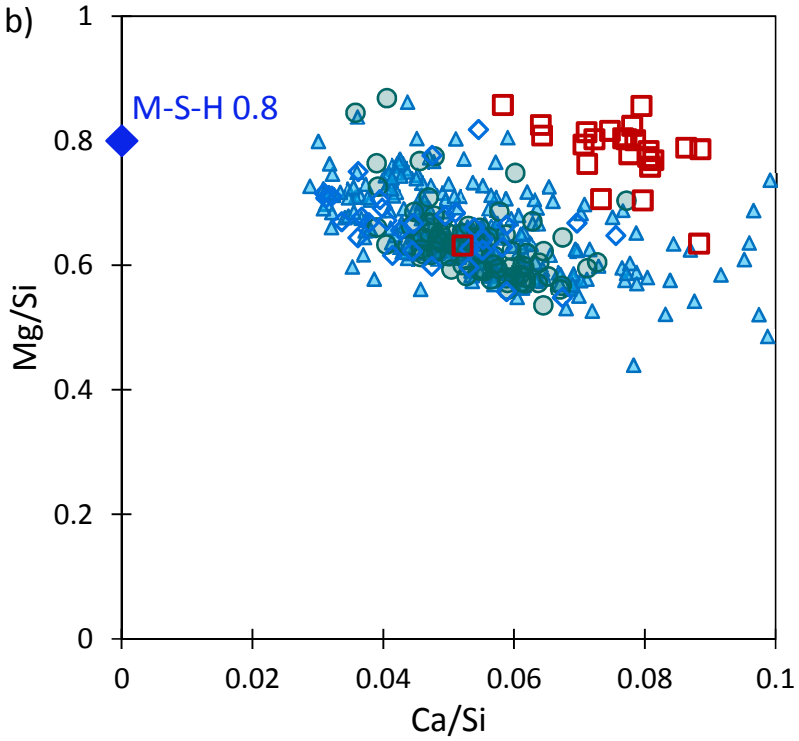


*Figure 5: a) Ca-Si-Mg ternary plots from EDS measurements of the M-S-H disk at 3 months, b) zoom on measured elemental ratios in M-S-H disk. Triangles= points in the entire disk, squares= high calcium content spots, circles= far from the interface, diamonds= close to the interface cf. Figure 2, empty red squares= results after 12 months.*

### 3.1.2. Liquid analysis

The changes in the reservoirs containing the solutions were followed. Figure 6 shows the pH values and the main species measured in solutions in the two reservoirs at t=0, after 3 and after 12 months. In addition traces of potassium and chloride were observed.

Initially, the solution in equilibrium with C-S-H contained mainly silicon (1.5 mmol/L), some calcium (0.8 mmol/L), no sodium (<0.003 mmol/L) and had a measured pH of 10.5. With time a decrease of pH was observed together with a small increase of the silicon and calcium concentrations. In addition, some sodium diffused from the M-S-H reservoir through the M-S-H and C-S-H disk. The increase of dissolved silicon in the C-S-H reservoir and the pH decrease with time were consistent with a

decalcification of C-S-H (L'Hôpital et al., 2016; Lothenbach and Nonat, 2015) confirming the EDS observations at the interface.

The solution in contact with M-S-H had initially a pH of 8.5 and contained 2.0 mmol/L silicon, 0.1 mmol/L of magnesium and 0.3 mmol/L sodium. After 3 months, a migration of calcium from the C-S-H side to the M-S-H solution was observed, while the pH increased from 8.5 initially to 9.3 after 3 months and to 9.6 after 12 months. The dissolved magnesium concentrations decreased from initially 0.1 mmol/L to <0.01 mmol/L as pH increased, This decrease of magnesium concentration at higher pH is consistent with results from batch experiments (Bernard et al., submitted; Bernard et al., 2017a; Bernard et al., 2017b; Nied et al., 2016).

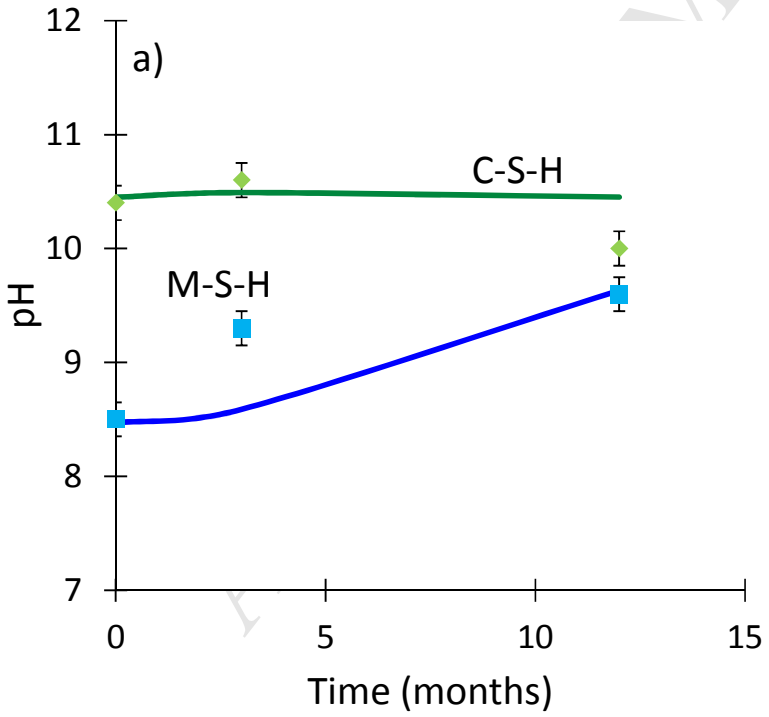

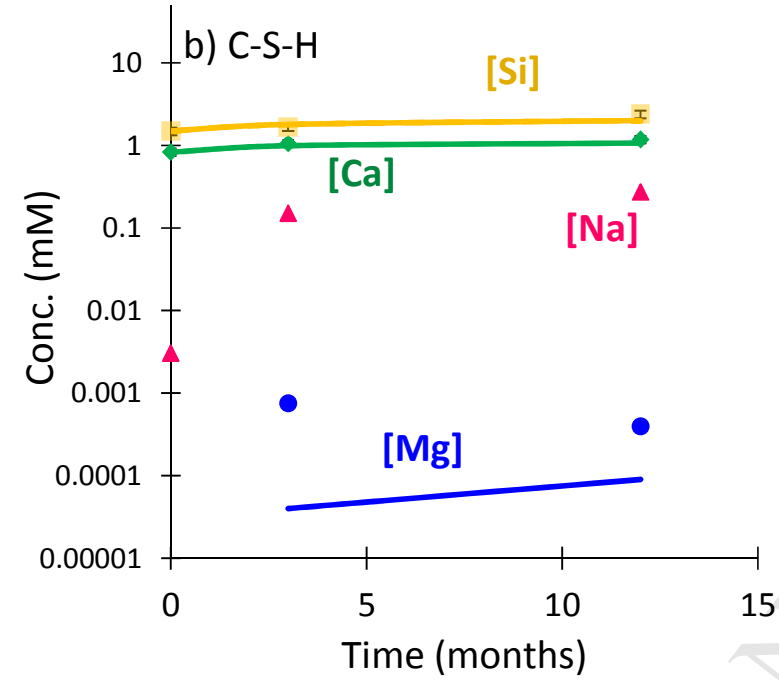


296

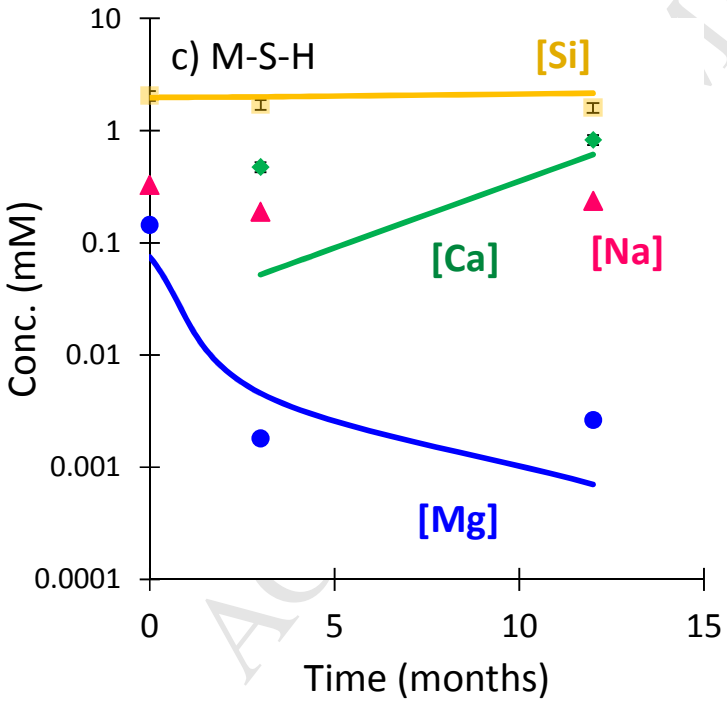


297

298 *Figure 6: Chemical evolutions of the reservoir chemistry (symbols) in parallel their modellings (solid lines: modelled*
299 *changes) as function of time. a) pH of the both solutions; b) Si, Ca, Na and Mg concentration in the C-S-H reservoir; c)*
300 *idem in the M-S-H reservoir ($[K]_{exp}$ and $[Cl]_{exp}$ < 0.05mmol/L).*

301

The occurrence of calcium in the M-S-H reservoir indicated that calcium diffused within 3 months completely through the M-S-H disk, in agreement with the homogeneous distribution of calcium in the M-S-H disk as observed by EDS. The pH of 9.5 in the M-S-H reservoir was below the range of stability of the C-S-H as already observed in (Bernard et al., submitted) which was consistent with the absence of C-S-H precipitation in the M-S-H disk.

In summary, the interaction of C-S-H with the M-S-H reservoir decreased the pH, and led to the decalcification of C-S-H and the precipitation of M-S-H. In contrast to C-S-H, M-S-H remained stable and took up a small amount of calcium.

### 3.2. Modelling of the chemical evolution of the interface

Reactive transport modelling assuming thermodynamic equilibrium was used to better understand the underlying mechanisms.

The C-S-H disk used in the calculations contained C-S-H with a Ca/Si of 0.8 and traces of C-S-H with a Ca/Si of 0.67 resulting in a pH value of 10.5. The disk of M-S-H was constituted of M-S-H with Mg/Si=0.83 and with Mg/Si=0.78 to obtain M-S-H with a Mg/Si of 0.8 as used experimentally and a pH of 8.5. The two disks had initially a total Ca/Si equal to 0.80 or Mg/Si equal to 0.80. The initial configuration and the solid compositions of the modelling are detailed in Figure 7a. The solution compositions of the reservoirs were set to the experimental solution compositions as given in Figure 7b. The pore solutions in the disks calculated by modelling agreed well with the solution composition reservoir as visible in the pH values. The measured calcium was with 0.83 mmol/L slightly lower than the 1.09 mmol/L in the modelled pore solution, while the measured modelled magnesium (0.07 mmol/L)

agreed well. The silicon concentrations of the reservoirs differed slightly within ± 0.6 mmol/L from the modelled pore solution of the disks.

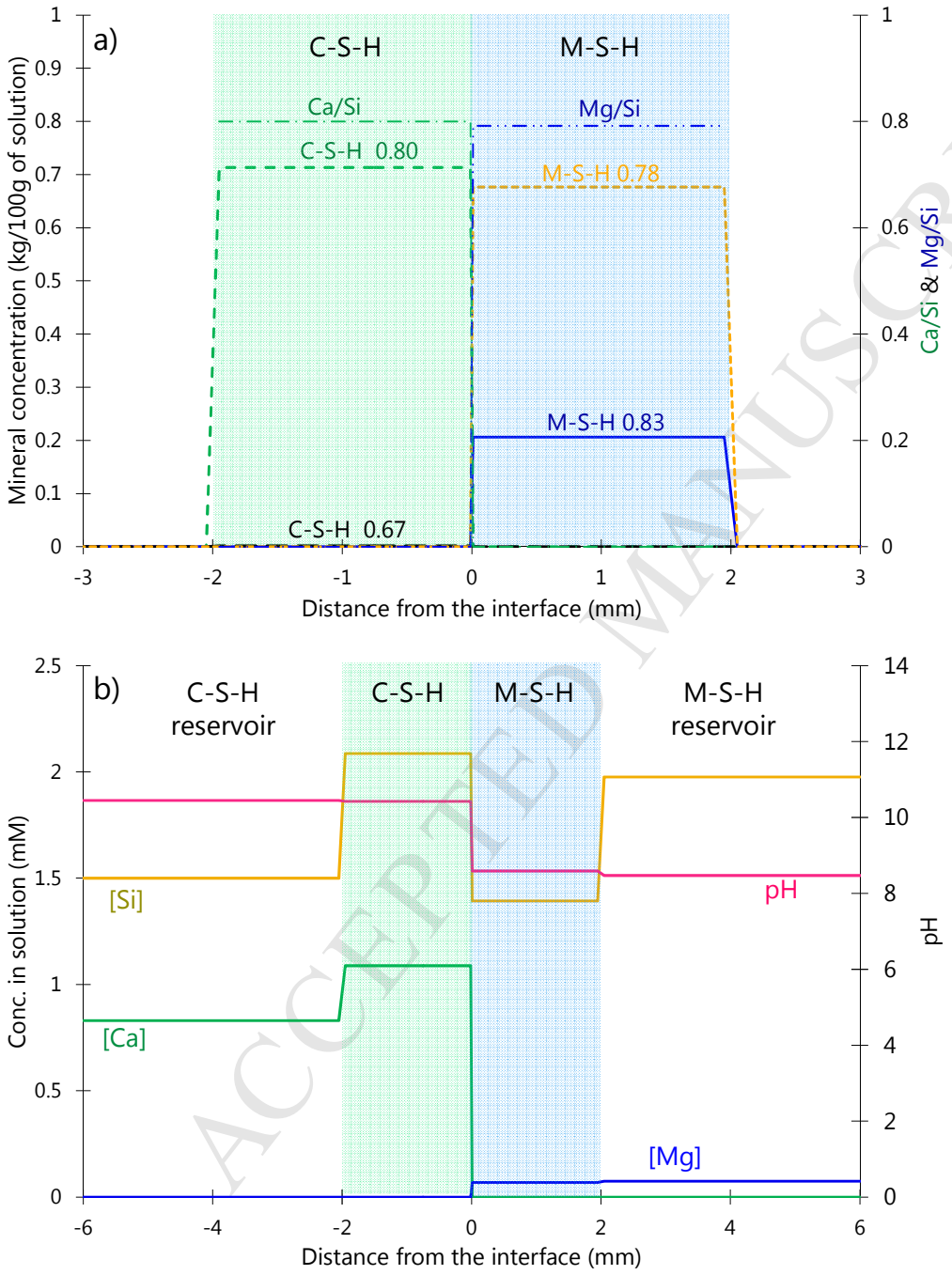


*Figure 7: Modelling of the initial state of the mineral concentration at the C-S-H 0.8 / M-S-H 0.8 interface.*

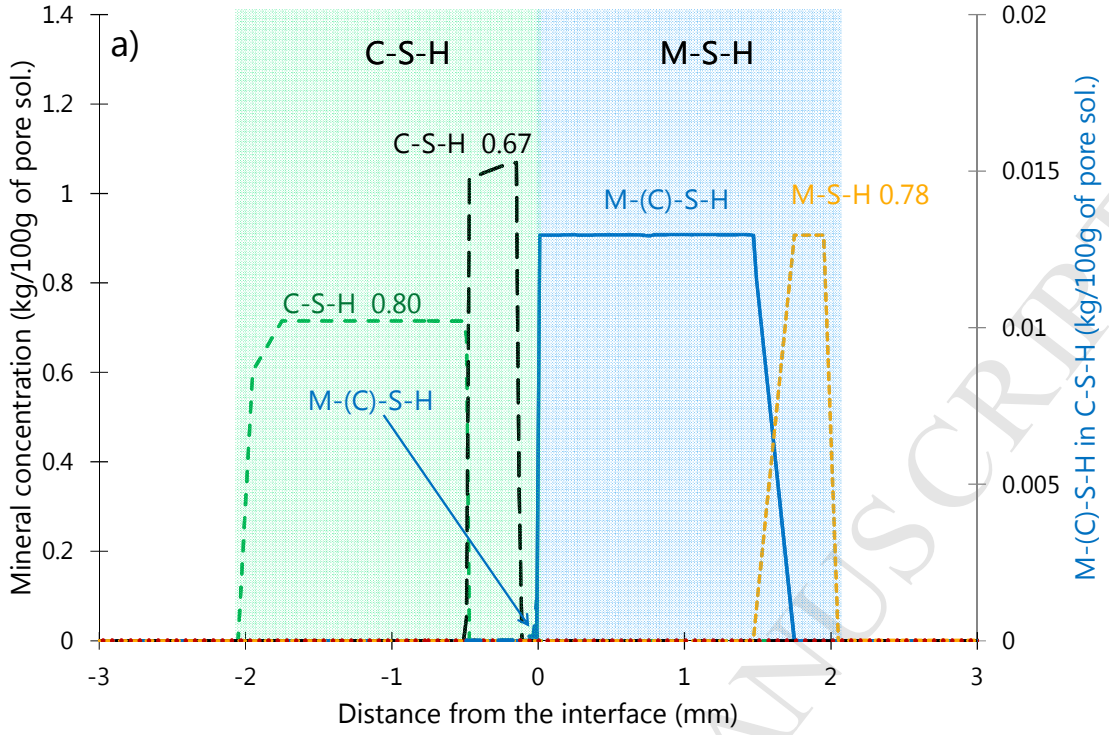


328

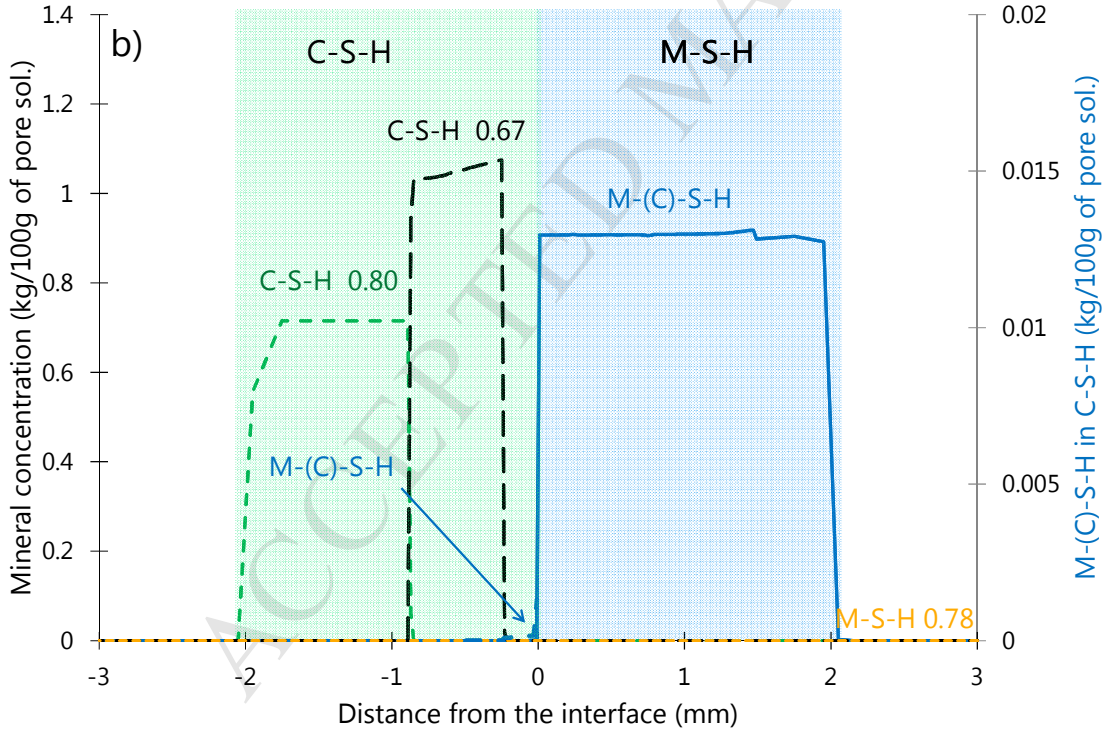


329

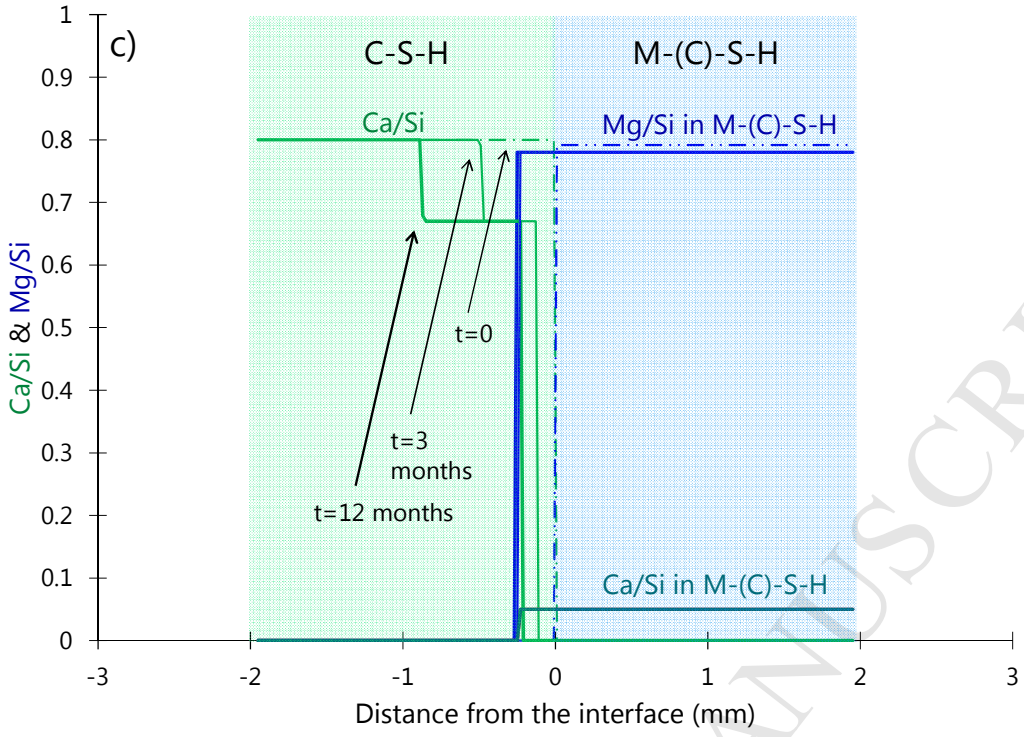


330

331 *Figure 8: Modelling of the main phases' evolution with M-S-H, M-(C)-S-H and C-S-H phases a) after 3 months, b) 12*
332 *months of interaction at the C-S-H / M-S-H interface at 25°C and c) the evolution of the molar ratios in the phases with*
333 *time.*

334

335 The modelling results after 3 and 12 months are summarized in Figure 8. They indicated decalcification
336 of the C-S-H disk in contact with the M-S-H disk near to the interface where the Ca/Si dropped from 0.8
337 to 0.67 while no amorphous silica was predicted. With time the decalcification front was calculated to
338 move further away from the interface. The modelling indicated a loss of silicon and calcium from the C-
339 S-H side to the M-S-H side as detailed in Figure 9. Twice as much calcium as silicon loss was predicted
340 by the modelling. On the opposite direction, a very low amount of magnesium diffused from the M-S-H
341 disk into the C-S-H side as shown in Figure 9. The very low amount of magnesium which is due to the
342 very low concentration of magnesium (Figure 7) imposed by the pH values of the system. Thus the
343 magnesium diffusion resulted in the formation of only a small quantity of M-(C)-S-H in the C-S-H disk

(Figure 8 and Figure 10). In the M-S-H disk, the M-S-H present initially was calculated to be destabilized while M-S-H containing some calcium, M-(C)-S-H, was calculated to form. After 3 months in the major parts of the M-S-H disk and after 12 months over the whole disk.

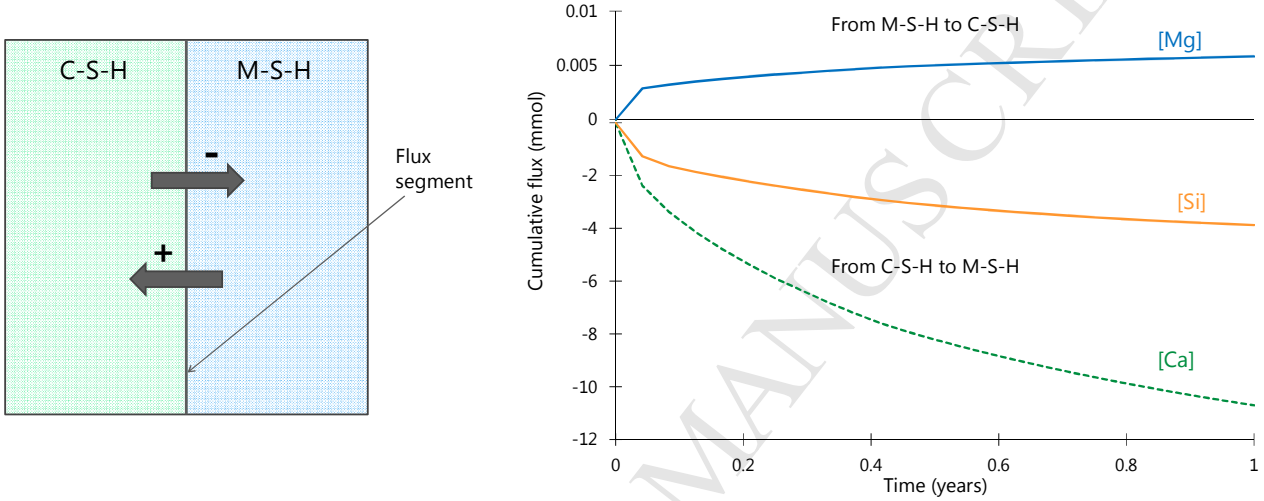


*Figure 9: Modelling of the cumulative flux at the C-S-H/M-S-H interface.*

After 12 months, the depth increased where M-(C)-S-H formation in the C-S-H disk was calculated. The modelling predicted the loss of silicon at the interface through diffusion and thus, a strong increase of porosity in the area where all C-S-H 0.67 was dissolved, while experimentally a limited increase of the porosity was observed and the formation of much more M-(C)-S-H.

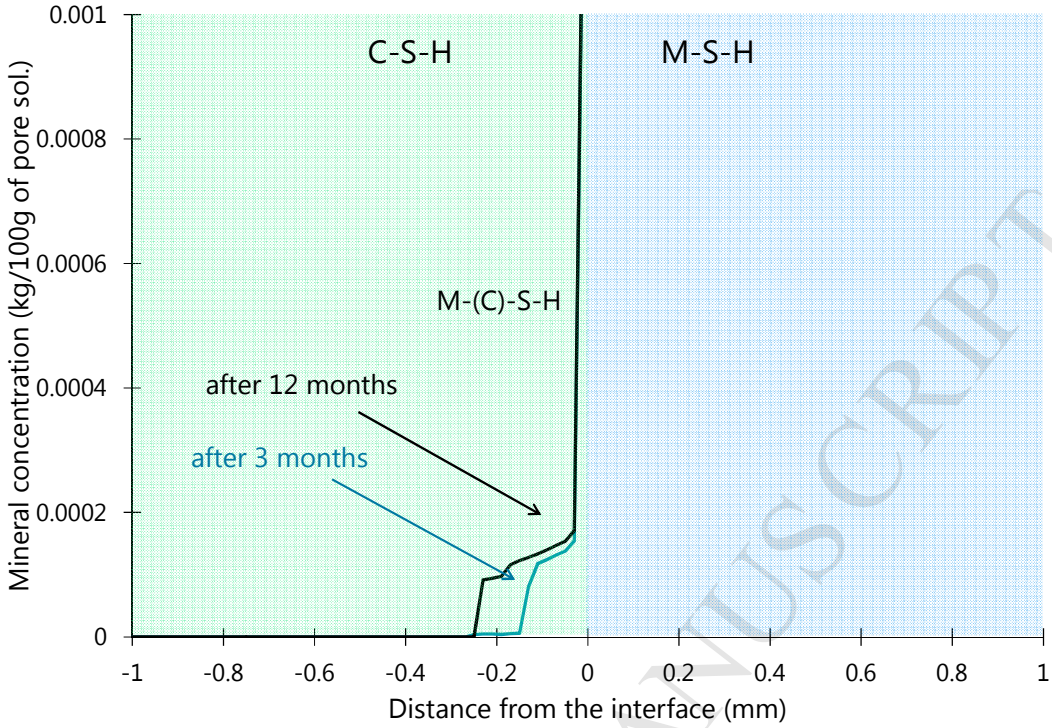


*Figure 10: Modelling with M-S-H, M-(C)-S-H and C-S-H phases of the M-S-H phases' evolution inside the C-S-H disk after 3 months and 12 months of interaction at the C-S-H/M-S-H interface at 25°C.*

The general phenomena observed experimentally, i.e. the decalcification of the C-S-H, the increasing porosity at the interface, the precipitation of M-S-H in the C-S-H disk and the uptake of calcium in the M-S-H phase were well described by the modelling.

Also the extent of degradation in the both materials was more or less consistent with the experimental results even this was not the aim of these experiments. After 3 months, the decrease of Ca/Si in C-S-H from 0.8 to 0.67 is with 490 µm calculated to be somewhat deeper than the 200 µm observed experimentally. However, after 12 months a good agreement between modelled and experimental data was obtained. Also the calculated depths of M-(C)-S-H formation in the C-S-H disk of 230 µm agreed with the experimental observation after 1 year, while after 3 months the calculated progress of 130 µm was further than the experimental observations. The main differences to the experiments were the much

lower amount of M-(C)-S-H calculated and the nearly complete dissolution of the zone at the interface. Both were related to the very low amount of magnesium transported in the calculations from the M-S-H disk into the C-S-H.

The reservoirs filled with the respective solutions were used in order to maintain the disks water saturated and to be able to observe the changes in the solution during the experiments. The modelling of the changes in the solutions is depicted in Figure 6 by the solid lines. With time, the calcium concentrations and the pH values increased in the M-S-H solution while the dissolved magnesium was calculated to decrease. The trends were in good agreement with the experimental observations. The modelled concentrations of silicon change little with time, while experimentally they decreased slightly. Also the changes in the C-S-H reservoir were well described by the modelling, which predicted an increase of calcium and silicon concentrations and little change in the pH values, while the experimental data after 12 months showed a slight decrease of the pH. The slight decrease of the measured pH in the C-S-H solution could be due to a small carbonation of the system which was not been taken into account in the modelling.

The modelling has also been carried out neglecting the uptake of calcium in M-S-H which gave similar results (see Appendix C) with the exception that no calcium uptake in the M-S-H disk was predicted.

## 4. Conclusions

Both experimental observations and reactive transport calculations of the cell experiments showed the partial destabilization of C-S-H in the presence of M-S-H within a few months. Experimentally, C-S-H was decalcified (drop of Ca/Si from 0.8 to 0.6±0.1) followed by the formation of amorphous silica and increased porosity. In addition, the precipitation of M-S-H was already observed after 3 months in the place where originally C-S-H were present. No incorporation of magnesium was observed in sound C-S-

392 H phase in agreement with observations in batch experiments (Bernard et al., submitted). Magnesium
393 was observed near the interface together with silicon only.

394 These simple cell experiments clearly proved that M-S-H formation occurs within a relatively short time
395 and that M-S-H forms from the dissolution of C-S-H, as had been postulated in (Dauzères et al., 2016;
396 Jenni et al., 2014; Lerouge et al., 2017; Mäder et al., 2017) based on field observations. In contrast to
397 such field studies, where the experimental differentiation between M-S-H and the clay minerals was
398 difficult, the absence of clay minerals in the present study and the clear separation of C-S-H and M-S-H
399 at the beginning of the diffusion experiments, allowed an unbiased interpretation of the results.

400 Calcium available from the dissolution of C-S-H was observed to diffuse into the M-S-H, where calcium
401 was partially bound to M-S-H. This agrees with the calcium uptake in M-S-H observed in batch
402 experiments (Bernard et al., submitted).

403 The good agreement between thermodynamic modellings and experiments underlined the applicability
404 of transport modelling to study deterioration of cementitious material in contact with claystone. The
405 magnesium perturbation can be added to the leaching, carbonation, or sulfate uptake in a more complete
406 modelling of in-situ studies.

407 Further steps for a better understanding of the formation of M-S-H would be to consider the possible
408 aluminum and alkali uptake in M-S-H and the effect of porosity on the diffusion of magnesium and
409 other ions.

410

411

412

## Acknowledgements

The authors would like to thank Isabelle Pochard, Céline Cau-dit-Coumes and Catherine Lerouge for helpful discussions.

## References

Bach, T., Chabas, E., Pochard, I., Cau Dit Coumes, C., Haas, J., Frizon, F., Nonat, A., 2013. Retention of alkali ions by hydrated low-pH cements: Mechanism and $Na^+/K^+$ selectivity. Cement and Concrete Research 51, 14-21.

Bernard, E., Lothenbach, B., Cau-Dit-Coumes, C., Chlique, C., Dauzères, A., Pochard, I., submitted. Magnesium and calcium silicate hydrates, Part I: Investigation of the possible magnesium incorporation in calcium silicate hydrate (C-S-H) and of the calcium in magnesium silicate hydrate (M-S-H). Applied Geochemistry.

Bernard, E., Lothenbach, B., Le Goff, F., Pochard, I., Dauzères, A., 2017a. Effect of magnesium on calcium silicate hydrate (C-S-H). Cement and Concrete Research 97, 61-72.

Bernard, E., Lothenbach, B., Rentsch, D., Pochard, I., Dauzères, A., 2017b. Formation of magnesium silicate hydrates (M-S-H). Physics and Chemistry of the Earth, Parts A/B/C 99, 142-157.

Berner, U., 1992. Evolution of pore water chemistry during degradation of cement in a radioactive waste repository environment. Waste Management 12, 201-219.

Brew, D.R.M., Glasser, F.P., 2005. Synthesis and characterisation of magnesium silicate hydrate gels. Cement and Concrete Research 35, 85-98.

Cau Dit Coumes, C., Courtois, S., Nectoux, D., Leclercq, S., Bourbon, X., 2006. Formulating a low-alkalinity, high-resistance and low-heat concrete for radioactive waste repositories. Cement and Concrete Research 36, 2152-2163.

Codina, M., 2007. Les bétons bas pH-Formulation, caractérisation et étude à long terme. INSA de Toulouse.

Codina, M., Cau-dit-Coumes, C., Le Bescop, P., Verdier, J., Ollivier, J., 2008. Design and characterization of low-heat and low-alkalinity cements. Cement and Concrete Research 38, 437-448.

Dauzères, A., Achiedo, G., Nied, D., Bernard, E., Alahrache, S., Lothenbach, B., 2016. Magnesium perturbation in low-pH concretes placed in clayey environment - solid characterizations and modeling. Cement and Concrete Research 79, 137-150.

Dauzères, A., Le Bescop, P., Cau-Dit-Coumes, C., Brunet, F., Bourbon, X., Timonen, J., Voutilainen, M., Chomat, L., Sardini, P., 2014. On the physico-chemical evolution of

low-pH and CEM I cement pastes interacting with Callovo-Oxfordian pore water under its in situ $CO_2$ partial pressure. Cement and Concrete Research 58, 76-88.
Fernández, R., Torres, E., Ruiz, A.I., Cuevas, J., Alonso, M.C., Calvo, J.L.G., Rodríguez, E., Turrero, M.J., 2017. Interaction processes at the concrete-bentonite interface after 13 years of FEBEX-Plug operation. Part II: Bentonite contact. Physics and Chemistry of the Earth, Parts A/B/C.
Garcia Calvo, J.L., Hidalgo, A., Alonso, C., Fernández Luco, L., 2010. Development of low-pH cementitious materials for HLRW repositories: Resistance against ground waters aggression. Cement and Concrete Research 40, 1290-1297.
Hong, S.-Y., Glasser, F., 1999. Alkali binding in cement pastes: Part I. The CSH phase. Cement and Concrete Research 29, 1893-1903.
Hummel, W., Berner, U., Curti, E., Pearson, F.J., Thoenen, T., 2002. Nagra/PSI Chemical Thermodynamic Data Base 01/01. Universal Publishers/uPUBLISH.com, USA, also published as Nagra Technical Report NTB 02-16, Wettingen, Switzerland.
Jenni, A., Mäder, U., Lerouge, C., Gaboreau, S., Schwyn, B., 2014. In situ interaction between different concretes and Opalinus clay. Physics and Chemistry of the Earth, Parts A/B/C 70, 71-83.
Kulik, D.A., 2011. Improving the structural consistency of CSH solid solution thermodynamic models. Cement and Concrete Research 41, 477-495.
L'Hôpital, E., Lothenbach, B., Kulik, D., Scrivener, K., 2016. Influence of calcium to silica ratio on aluminium uptake in calcium silicate hydrate. Cement and Concrete Research 85, 111-121.
Lerouge, C., Gaboreau, S., Grangeon, S., Claret, F., Warmont, F., Jenni, A., Cloet, V., Mäder, U., 2017. In situ interactions between Opalinus Clay and Low Alkali Concrete. Physics and Chemistry of the Earth, Parts A/B/C 99, 3-21.
Lothenbach, B., Le Saout, G., Ben Haha, M., Figi, R., Wieland, E., 2012. Hydration of a low-alkali CEM III/B–SiO2 cement (LAC). Cement and Concrete Research 42, 410-423.
Lothenbach, B., Nied, D., L'Hôpital, E., Achiedo, G., Dauzères, A., 2015. Magnesium and calcium silicate hydrates. Cement and Concrete Research 77, 60-68.
Lothenbach, B., Nonat, A., 2015. Calcium silicate hydrates: Solid and liquid phase composition. Cement and Concrete Research 78, 57-70.
Lothenbach, B., Rentsch, D., Wieland, E., 2014. Hydration of a silica fume blended low-alkali shotcrete cement. Physics and Chemistry of the Earth, Parts A/B/C 70, 3-16.
Mäder, U., Jenni, A., Lerouge, C., Gaboreau, S., Miyoshi, S., Kimura, Y., Cloet, V., Fukaya, M., Claret, F., Otake, T., Shibata, M., Lothenbach, B., 2017. 5-year chemico-physical evolution of concrete-claystone interfaces. Swiss Journal of Geosciences 110, 307-327.

Nied, D., Enemark-Rasmussen, K., L'Hopital, E., Skibsted, J., Lothenbach, B., 2016. Properties of magnesium silicate hydrates (MSH). Cement and Concrete Research 79, 323-332.

Pearson, F.J., Arcos, D., Bath, A., Boisson, J.-Y., Fernandez, A.M., Gäbler, H.-E., Gaucher, E., Gautschi, A., Griffault, L., Hernan, P., Waber, H.N., 2003. Mont-Terri Project – Geochemistry of Water in the Opalinus Clay Formation at the Mont Terri Rock Laboratory. Reports of the FOWG, Geology Series 5, 319.

Poyet, S., Le Bescop, P., Cau Dit Coumes, C., Touzé, G., Moth, J., 2014. Formulating a low-alkanity and self-consolidating concrete for the DOPAS-FSS experiment. NUWCEM, 2nd international symposium on cement-based materials for nuclear waste, Avignon, France.

Van der Lee, J., 1998. Thermodynamic and mathematical concepts of CHESS. Technical Report Nr LHM/RD/98/39 Ecole des Mines de Paris, Fontainebleau, France.

Van Der Lee, J., De Windt, L., Lagneau, V., Goblet, P., 2003. Module-oriented modeling of reactive transport with HYTEC. Computers & Geosciences 29, 265-275.

Walker, C.S., Sutou, S., Oda, C., Mihara, M., Honda, A., 2016. Calcium silicate hydrate (CSH) gel solubility data and a discrete solid phase model at 25° C based on two binary non-ideal solid solutions. Cement and Concrete Research 79, 1-30.

Highlights:

- C-S-H is destabilized at pH values below 10
- M-S-H forms from the dissolution of C-S-H and dissolved magnesium
- Calcium uptake occurs in M-S-H
- Good agreement of the reactive transport modelling with the changes experimentally observed